

Physics Extended Essay

An Investigation of the Aerodynamic Effects of Fin-Length-to-Diameter Ratio on Spherical
Projectiles' Range and Velocity Decay

May 2025

MLA 8

Table of Contents

1. Research Question.....	4
2. Introduction.....	4
3. Background Research.....	5
3.1 Projectile Motion.....	5
3.2 Drag.....	5
3.3 Fins and Aerodynamic Stability.....	6
3.3.1 Horizontal Range.....	7
3.3.2 Velocity Decay.....	8
3.4 Effect of Fins on Projectile Motion.....	10
3.5 Consideration of Alternative Methodologies and Assumptions.....	12
4. Hypothesis.....	13
5. Variables.....	13
5.1 Independent Variable.....	13
5.2 Dependent Variables.....	14
5.3 Control Variables.....	15
5.4 Safety Precautions.....	15
5.5 Environmental and Ethical Considerations.....	16
6. Materials Used.....	16
7. Experimental Procedure.....	16
7.1 Preliminary Trials and Challenges.....	16
7.2 Schematic & Actual Setup.....	18
7.3 Procedure.....	19
8. Data Collection.....	20
8.1 Raw data.....	20
8.1.1 Uncertainties in Horizontal Range.....	21
8.2 Processed Data.....	23
8.2.1 Uncertainties in Velocity Decay.....	26
9. Analysis.....	27

9.1 Horizontal Range.....	27
9.2 Investigation of 0.75x and 1.00x outliers.....	28
9.3 Theoretical vs. Experimental Comparisons.....	30
9.4 Velocity decay.....	32
10. Evaluation.....	36
10.1 Limitations.....	36
10.2 Systematic Errors.....	37
10.3 Random Errors.....	37
11. Conclusion.....	38
12. Further Extension.....	38
13. Works Consulted.....	39
14. List of Figures.....	42
15. Appendix.....	43
15.1 Maximum Velocity.....	43
15.2 Python Code for Graph 9.1.....	44
15.3 Python Code for Graph 9.4.....	45
15.4 Python Code for Figure 9.4.....	46
15.5 Experimental Setup.....	47
15.6 Uncertainty Calculations.....	47
15.7 Secondary Sources.....	49

1. Research Question.

To what extent does Fin-Length-to-Diameter Ratio affect the horizontal range and velocity decay of a spherical projectile under the influence of air resistance?

2. Introduction.

Projectile motion describes the path an object takes when launched under the influence of gravity. In an ideal environment, i.e. a vacuum, the motion is predictable and parabolic; however, in real-word, air resistance significantly affects the projectile's trajectory. In this investigation, I explore the aerodynamic effects of fin length on spherical projectiles. Specifically, I will examine how varying the fin length-to-diameter ratio impacts the horizontal range and velocity decay of a 250g steel sphere.

My experimental approach involves using a spring-loaded launcher and a high-speed camera (240 fps) to record the motion of projectiles fitted with fins of different lengths. The data is analyzed using Tracker software to determine velocity decay and horizontal range. I will then compare these results against theoretical models that neglect air resistance to quantify the extent to which the added fins affect the projectile's said parameters.

My study finds applications in aerospace. NASA's Orion and Russia's Soyuz capsules use aerodynamic surfaces to control re-entry angle and prevent tumbling. My fascination with subtle design changes in aerospace led to this investigation, which I hope will inspire further studies in spacecraft dynamics and re-entry engineering.

In the following sections, I will detail the experimental procedure and methodology, present and analyze the data, and discuss the implications of the findings. Ultimately, this EE is my personal journey into aerodynamics, and serves as a launchpad for my future studies in spacecraft dynamics and atmospheric re-entry technology.

3. Background Research.

3.1 Projectile Motion.

In an ideal scenario without air resistance, a projectile launched at speed v_0 and angle θ follows a parabolic path under gravity alone, with its horizontal range given by ("3.3: Projectile Motion."):

$$R_{\text{ideal}} = \frac{v_0^2 \sin(2\theta)}{g} \dots(1)$$

However, real projectiles do not travel in a vacuum; they experience air resistance, which lowers the actual distance traveled and increases velocity decay. Thus, real-world trajectories deviate significantly from their ideal parabolic trajectory.

3.2 Drag.

Air resistance, also referred to as drag, depends on the object's shape, size, velocity, and the fluid's density and viscosity. The equation for drag force is ("6.07: Drag Force and Terminal Speed") :

$$F_D = \frac{1}{2} C_d \rho A v^2 \dots(2)$$

where C_d is the drag coefficient, ρ is air density, A is cross-sectional area, and v is velocity. The drag coefficient (C_d) is a dimensionless number that quantifies how much an object resists motion through a fluid, depending on its shape, surface roughness, and flow conditions. Adding fins can substantially increase C_d ; studies (AIAA, 2020) also note a 15-25% rise in the drag coefficient for finned projectiles which lead to shorter flight distances and steeper velocity decays.

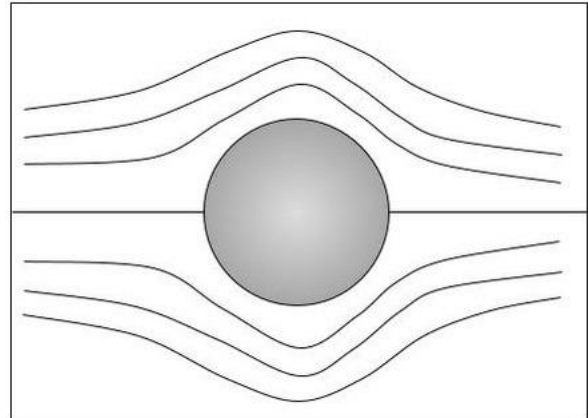


Figure 3.2 Flow of fluid around a sphere when there is relative motion between the fluid and the sphere.



Image 3.3 Vostok 5 re-entry vehicle (Vostok 5 Reentry Capsule 01.)

3.3 Fins and Aerodynamic Stability.

Most aerodynamic literature focuses on bullets or slender missiles, but spherical bodies such as re-entry capsules have different wake characteristics. A re-entry vehicle is a spacecraft or projectile designed to withstand extreme heat and aerodynamic forces while re-entering a planetary atmosphere at high velocity. Wake characteristics describe the airflow behavior behind a moving object, including turbulence, vortex formation, which impact drag, stability, and overall aerodynamic performance ("Vortex Shedding").

1. Turbulence

Turbulence is the irregular, and unpredictable movement of a fluid caused by rapid changes in velocity and pressure ("Laminar and Turbulent Flow"). It occurs when smooth (laminar) flow becomes unstable due to high speeds, or quick changes in direction. Turbulence increases drag and affects stability, making it crucial to control in aircraft and re-entry vehicles.

2. Vortex Formation

A vortex is a rotating swirl of fluid that forms when high-speed airflow moves around an object and separates from its surface ("Vortex"). This occurs when air or liquid moves faster on one side than the other, creating a low-pressure zone that causes the flow to spiral. Vortices can be seen behind in wake regions of projectiles, influencing lift, drag, and stability.

3.3.1 Horizontal Range.

In vacuum, a projectile maintains its horizontal velocity and thus achieves a maximum range given by (Homer et al. 31-2) in equation (1). Under drag, energy is lost to air resistance and this decreases the horizontal range. Fins greatly increase the cross-sectional area A , thus raising the drag force. Therefore, as fin length grows, we can expect a stronger reduction in horizontal range. In my experiment, the horizontal range is measured by marking the projectile's landing point under each fin configuration.

3.3.2 Velocity Decay

Beyond range reduction, drag also affects the velocity profile of a projectile over time. Under conditions without air resistance, horizontal velocity would remain nearly constant. However, drag causes velocity decay (deceleration), which can be shown mathematically by:

$$m \frac{dv}{dt} = -\frac{1}{2} C_d \rho A v^2 \quad \dots(3)$$

where m is the projectile's mass. Fins increase A (and often C_d), producing a larger deceleration $\frac{dv}{dt}$. In my EE, a 240fps camera tracks the projectile to determine how quickly velocity drops using Tracker. By plotting and comparing velocity decay, i.e. deceleration for different fin lengths, I aim to explore the relationship between fin length and velocity decay.

Derivation of Velocity Decay Equation with Quadratic Drag

Rearranging equation (3):

$$\frac{dv}{dt} = -\frac{C_d \rho A}{2m} v^2$$

Let:

$$k = \frac{C_d \rho A}{2m} \quad \dots(4)$$

so that:

$$\frac{dv}{dt} = -kv^2$$

Solving for $v(t)$ by rearranging the differential equation:

$$\frac{dv}{v^2} = -kdt$$

Integrating both sides:

$$\int \frac{dv}{v^2} = \int -kdt$$

$$\therefore -\frac{1}{v} = -kt + C$$

$$\therefore v(t) = \frac{1}{kt - C}$$

Applying the initial condition $v(0) = v_0$, we determine C :

$$C = \frac{1}{v_0}$$

Thus, the final equation for velocity decay due to quadratic drag is:

$$v(t) = \frac{v_0}{1 + kv_0 t} \dots (5)$$

where:

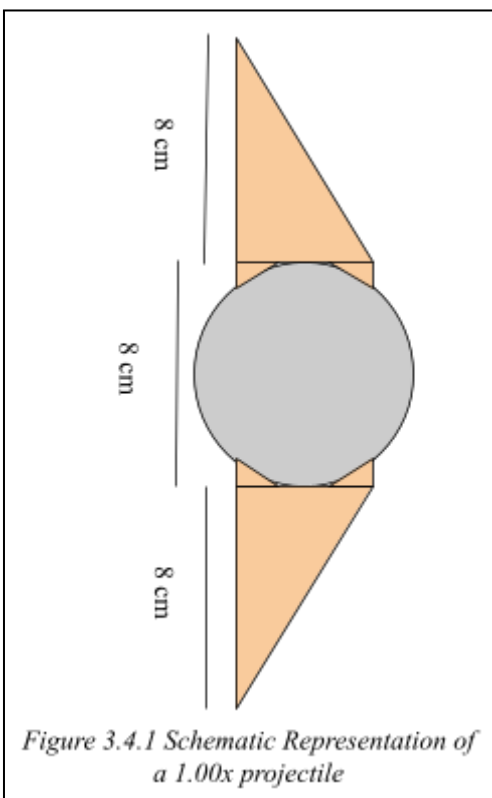
$$k = \frac{C_d \rho A}{2m}$$

The velocity decays inversely with time due to the quadratic nature of drag, and the rate of decay is determined by the drag coefficient C_d , which depends on fin design. I will compare this equation with my experimental velocity decay values to determine its validity.

3.4 Effect of Fins on Projectile Motion.

Fins are commonly used to stabilize projectiles. They affect the projectile motion by:

1. Increasing drag by increasing the surface area interacting with air.
2. Guiding airflow, thus improving aerodynamic stability by reducing projectile wobbling (Yin, Wu, and Lei) .



In my EE, two triangular cardboard fins will be symmetrically attached using an adhesive on opposite ends to the spherical projectile, which is an 8 cm long, 250g hollow steel sphere. The size chosen is according to the fin length-to-sphere diameter ratio. (for e.g., 0.50x means two 4 cm length fins attached at opposite ends). The fin length-to-diameter ratio is taken as a dimensionless parameter to ensure scalability and applicability across different projectile sizes. In aerospace engineering, this ratio is widely used in designing re-entry capsules, missiles, and aerodynamic bodies, as it allows for comparisons across different

scales without being limited to absolute measurements. For example, the Apollo Command Module and similar re-entry vehicles (ASME 1992) use similar proportional scaling to optimize stability and drag characteristics. Using this ratio ensures that the results from my experiment can be generalized and applied to spherical re-entry vehicles, regardless of their actual size.



The selection of eight fin lengths (0.00x - control, 0.25x, 0.50x, 0.75x, 1.00x, 1.25x, 1.50x, 1.75x, 2.00x relative to the sphere's diameter) allows for a thorough analysis of the relationship between fin length and aerodynamic performance, which can be seen in real-life aerospace vehicles. While re-entry vehicles and other aerospace objects are not perfectly spherical, the choice of a sphere approximates well for my case.

*Figure 3.4.2 Actual
Representation of a 1.00x
projectile*

3.5 Consideration of Alternative Methodologies and Assumptions.

Alternative Methodology	Description	Advantages	Disadvantages
CFD Simulations	Use computational fluid dynamics (i.e. ANSYS Fluent) to model air resistance and wake turbulence for different fin configurations (Yin, Wu, and Lei).	Precise modeling under conditions that can be controlled; can eliminate experimental inconsistencies.	Requires extensive computational power and expertise; less feasible in school laboratory.
Wind Tunnel Testing	Test projectiles in a controlled airflow to directly measure drag forces and turbulence.	Direct measurement of aerodynamic performance; provides information about drag force and turbulence.	Requires specialized equipment; may not accurately replicate real-world projectile motion with gravity and launch dynamics.
Ticker Tape Timer	Attach a ticker tape to the projectile so that as it moves, a mechanical timer marks the tape at regular intervals. The spacing between the marks can then be analyzed to approximate the projectile's velocity and acceleration.	Low-cost method that requires only basic equipment. Provides a straightforward way to visualize motion over time.	Less precise than digital video techniques and can introduce errors if the tape's movement is affected by external factors or if the tape attachment alters the projectile's motion.
Stroboscope Photography	A strobe light flashes at fixed intervals while a camera set for long exposure captures the projectile's flight. The resulting multiple images along the trajectory, spaced by known time intervals, allow calculation of range and velocity.	Relatively simple to set up compared to a digital video. Provides a clear visual record of motion without requiring advanced equipment.	The accuracy depends on the strobe's flash rate and the quality of the image captured and it is sensitive to ambient light.

Table 3.5.1 Alternative Methodologies

Assumption	Significance	Mitigation Strategy
Air resistance is the only external force aside from gravity	Neglecting external factors like wind and air density variations simplifies calculations but may introduce minor discrepancies.	Conducted trials indoors to minimize wind effects and ensured consistent environmental conditions.
Negligible projectile spin (no Magnus effect)	Spin could alter the trajectory due to lift forces, affecting velocity decay and range (Yin, Wu, and Lei).	Calibrated launch mechanism to minimize spin and visually inspected launches for consistency during preliminary trials.
Fins are perfectly rigid and symmetrically attached	Slight bending or misalignment of fins could introduce variations in drag experienced.	Carefully measured and attached fins using an adhesive on the same marked spots for each projectile to ensure uniformity.
Camera tracking system is perfectly accurate	Tracking software may have frame rate inconsistencies, affecting velocity decay calculations.	Used a high-frame-rate camera and calibrated the software with a known calibration stick.

Table 3.5.2 Assumptions

4. Hypothesis.

It is hypothesised that increasing the fin lengths on a spherical projectile will lead to greater velocity decay and a reduction in horizontal range due to increased aerodynamic drag force experienced due to the addition of fins.

5. Variables.

5.1 Independent Variable.

Fin-Length-to-Diameter Ratio: 0.25x, 0.50x, 0.75x, 1.00x, 1.25x, 1.50x, 1.75x, 2.00x fin lengths relative to the sphere's diameter.

5.2 Dependent Variables.

Velocity Decay: Measured using video camera tracking and then using Tracker to analyse motion.

Horizontal Range: Measured from the launch point to the landing point to determine how air resistance affects projectile distance.

My rationale for investigating these is that horizontal range provides a clear endpoint measure of how far the projectile travels before landing, and thus is an integration of all its aerodynamic influences over the entire flight. However, range alone does not reveal how quickly the projectile slows down at each moment, which is where velocity decay becomes essential. By tracking the deceleration, i.e. the velocity decay, we gain insight into how drag forces act at different stages of the trajectory.

In real-world aerospace applications, both distance and deceleration rates are necessary. For instance, a re-entry capsule's landing zone (range) must be accurately predicted, but the rate of velocity loss (velocity decay) also dictates stability and crew safety. By measuring range and velocity decay together, I gain a more comprehensive understanding of the aerodynamic effects at work and ensure that my conclusions apply more broadly to practical problems.

5.3 Control Variables

Control Variable	Reason for Control	Method of Control
Initial Launch Speed	Ensures variations in dependent variables are due to aerodynamic factors, not speed changes.	A spring-loaded mechanical launcher or consistent manual force will be calibrated and used.
Launch Angle (θ)	Affects range and trajectory shape, so it must remain constant.	Fixed at 45° using a protractor and an angle-adjustable ramp.
Mass of the Projectile (m)	Ensures differences in motion are due to aerodynamic effects, not inertia changes.	All projectiles are identical spheres of the same steel material and 250 g weight.
Projectile Material	Different materials may affect surface friction, and air resistance.	All projectiles are made of the same steel material to ensure uniform properties.
Projectile Spin and Orientation	Spin can introduce the Magnus effect, altering trajectory.	Launched without intentional spin by ensuring a consistent initial orientation.
Launch Mechanism	Prevents inconsistencies in initial force and projectile release.	A controlled launcher and a consistent manual release method is used.
Measurement Equipment	Ensures consistent data collection and avoids systematic errors.	Same high-speed camera is used for all trials.
Measurement Reference Points	Eliminates discrepancies in distance and height recordings.	The starting point of measurement is always the same .
Environmental Conditions	Wind or temperature changes could alter drag and trajectory.	Experiment conducted indoors to eliminate external disturbances.

Table 5.3 Control Variables

5.4 Safety Precautions

The launch setup should be stable, and all tests should be conducted away from people and fragile objects. Wear safety goggles to prevent eye injuries, and the testing area should remain clear to avoid accidental collisions.

5.5 Environmental and Ethical Considerations.

Minimize environmental impact by reusing projectiles across multiple trials and using biodegradable cardboard fins instead of plastic. Indoor testing reduces wind interference.

6. Materials Used

Item	Purpose	Quantity
250g Steel Sphere (8cm Diameter)	Projectile for launch and testing	8
Cardboard Fins (Various Sizes)	Modifying aerodynamic properties of the sphere	10 (2 per fin length)
High-Speed Camera	Capturing projectile's motion for input into Tracker	1
Tracker Software	Analyzing velocity decay	1
Metre rule ($\pm 0.001\text{m}$)	Measuring horizontal range	As required
Digital Scale ($\pm 0.01\text{g}$)	Measuring mass of projectiles	1
Tripod	Stabilizing camera for accurate video capture	1
Launch Apparatus	Provide consistent launch conditions. A spring-loaded mechanical launcher attached to a ramp system. The spring is calibrated for consistent force and therefore, same initial velocity for all projectiles. Ramp is fixed at 45 degrees for maximum range using a protractor.	1

Table 6. Materials Used

7. Experimental Procedure.

7.1 Preliminary Trials and Challenges.

Before conducting the full experiment, preliminary trials were performed to assess the feasibility of the methodology, identify potential challenges, and refine data collection techniques.

Initially, thin cardboard fins bent under airflow, altering their angle of attack. The angle of attack is the angle between the direction of airflow and the surface of an object. Basically, the angle of attack is how much the fins are tilted relative to the airflow. If it changes unpredictably, it can affect the projectile's flight, causing instability.

Switching to thicker cardboard, helped reduce bending considerably. Visual inspection of the video in slow-motion confirmed that spin of the projectile is reduced. The projectiles were placed perpendicular on the launcher's body which was marked with the exact spot (fiducial marker). This made sure that no spin or tumbling effect occurred.

To ensure consistent launch conditions, the spring launcher was calibrated by controlling the compression distance of the spring. A fixed reference point was established on the launcher, marking the exact distance the spring needed to be compressed before each launch. A mechanical stopper was used to prevent over-compression and ensure that the spring was pulled back to the same position every time. A fixed marker was placed on the launcher to indicate the exact position where the spring needed to be compressed before release. This ensured that the same amount of stored energy was used each time. Several test launches were conducted to check for noticeable differences in projectile motion. My method ensured that the same amount of potential energy was stored in the spring for each trial and thus the same amount of force was applied leading to the same initial velocity for the projectiles, as they all weighed the same (250 g) and mass of fins was negligible.

7.2 Schematic & Actual Setup.

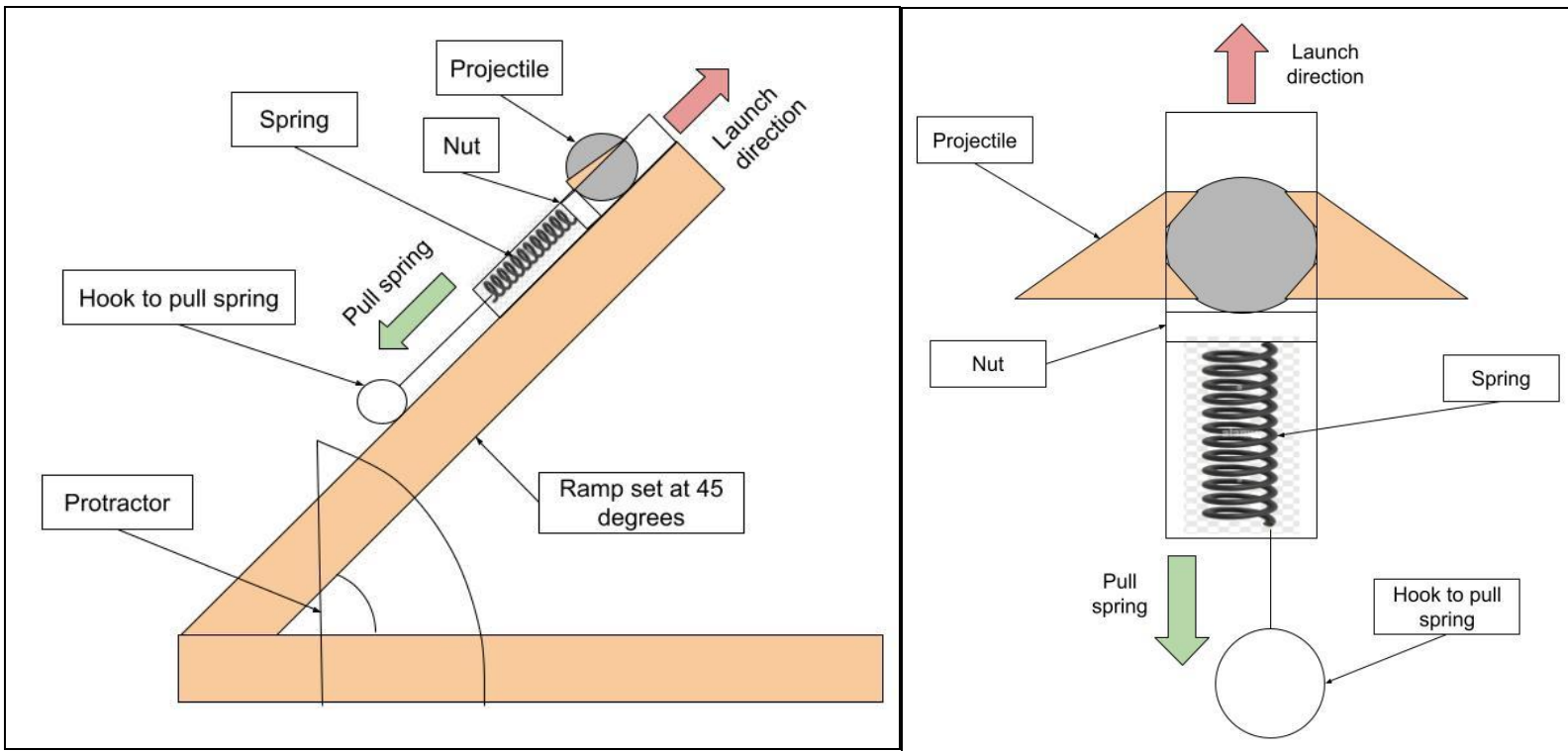


Figure 7.2.1 Schematic Representation of Experimental Setup

Figure 7.2.2 Top view of projectile placed in launcher

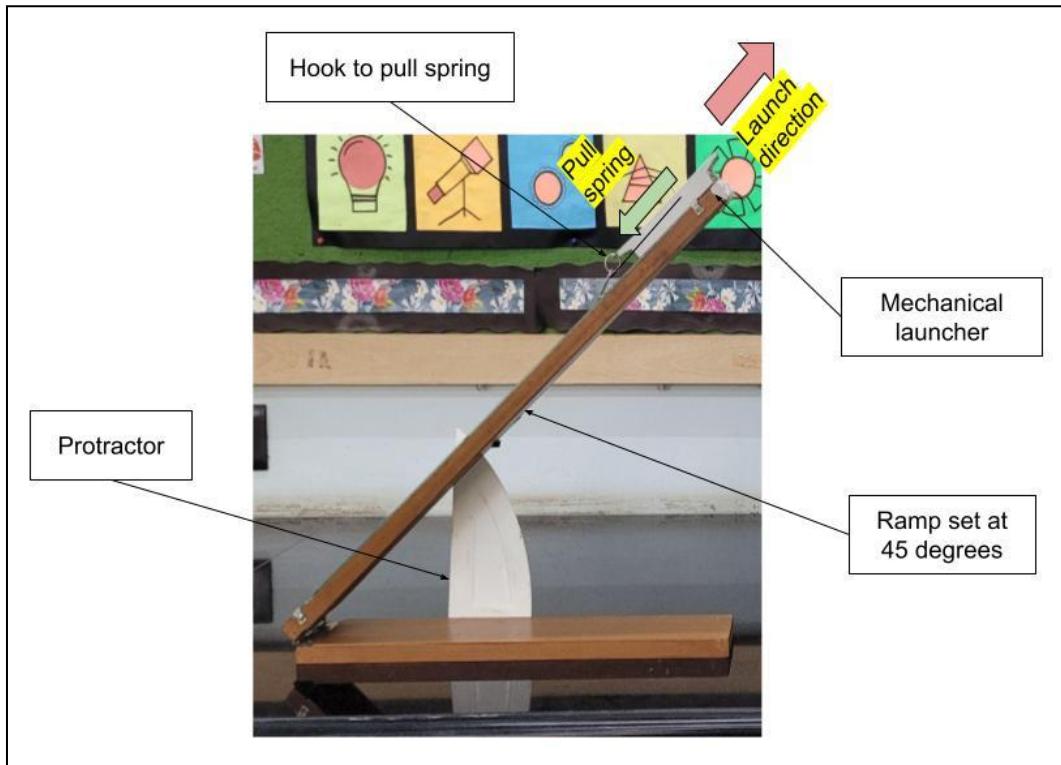


Figure 7.2.3 Actual Representation of Experimental Setup

7.3 Procedure.

1. Set up a spring-loaded launcher on a flat, level desk¹.
2. Fix a high-speed camera on a tripod at a fixed distance from the launch area, making sure it is aligned to capture the full projectile trajectory.
3. Mark launch point using metre rule(s).
4. Attach two cardboard fins of 0.25x ratio to the sphere using strong adhesive.
5. Load the 0.25x projectile into the launcher and set it at a fixed launch angle of 45°.
6. Launch the projectile and record the launch using the high-speed camera.
7. Conduct five trials per fin length under identical conditions.
8. Measure the horizontal range (impact point - launch point) using meter rule(s).
9. Import footage into Tracker, calibrate the scale, and mark the projectile's center of mass.
10. Extract velocity data and calculate velocity decay (rate of velocity loss).
11. Repeat the experiment for all fin lengths and the control.

¹ Note: Refer to [Appendix 15.5](#) for extended view of Experimental Setup

8. Data Collection.

8.1 Raw data.

Fin length-diameter ratio / L	Horizontal Range / R / m					
	Trial 1	Trial 2	Trial 3	Trial 4	Trial 5	Average
0.00	2.025	1.993	2.032	2.076	1.988	2.023
0.25	1.927	1.927	1.963	1.855	1.864	1.907
0.50	1.966	1.882	1.896	1.822	1.866	1.866
0.75	1.727	1.723	1.688	1.696	1.734	1.714
1.00	1.868	1.869	1.869	1.872	1.871	1.870
1.25	1.712	1.677	1.662	1.726	1.747	1.704
1.50	1.597	1.612	1.566	1.561	1.662	1.600
1.75	1.568	1.627	1.548	1.628	1.419	1.557
2.00	1.449	1.477	1.533	1.434	1.419	1.462

Table 8.1 Horizontal range

Sample Average Horizontal Range Calculation for 0.75x fin length:

$$\text{Average Horizontal Range} = \frac{\text{Trial 1} + \text{Trial 2} + \text{Trial 3} + \text{Trial 4} + \text{Trial 5}}{5}$$

$$\begin{aligned}\text{Average} &= \frac{1.727 + 1.723 + 1.688 + 1.696 + 1.734}{5} \\ &= \frac{8.568}{5} \\ &= 1.714 \text{ m}\end{aligned}$$

8.1.1 Uncertainties in Horizontal Range

The least count of an instrument provides the smallest measurable unit, but it does not account for the variations in repeated trials caused by random errors such as air turbulence, mechanical minor launch inconsistencies, or alignment differences. Thus, I chose standard deviation as a measure for my uncertainties as it is a more comprehensive measure of uncertainty as it quantifies the spread of data around the mean and captures the actual experimental variability rather than just instrument precision.

To calculate the uncertainty, the standard deviation of the mean (standard error) formula is used:

$\sigma_{\text{mean}} = \frac{\sigma}{\sqrt{N}}$ where: σ_{mean} is the uncertainty in the average value, σ is the standard deviation of the data set and N is the number of trials (in my case, $N = 5$).

The uncertainties for the average values are calculated and given below:

Fin length-diameter ratio / L	Average Horizontal Range / R / m	Standard Deviation / Δ m
0.00	2.02	0.04
0.25	1.91	0.05
0.50	1.87	0.05
0.75	1.71	0.02
1.00	1.87	0.00
1.25	1.70	0.04
1.50	1.60	0.04
1.75	1.56	0.09
2.00	1.46	0.05

Table 8.1.1 Standard Deviation as Uncertainty

Sample Standard Deviation Calculation for 0.75x fin length:

Given data: $x_1 = 1.727$, $x_2 = 1.723$, $x_3 = 1.688$, $x_4 = 1.696$, $x_5 = 1.734$

1: Calculate the mean \bar{x} :

$$\bar{x} = \frac{x_1 + x_2 + x_3 + x_4 + x_5}{5} = \frac{1.727 + 1.723 + 1.688 + 1.696 + 1.734}{5} \approx 1.714 \text{ m}$$

2: Calculate each deviation from the mean and square it:

$$(x_1 - \bar{x})^2 = (1.727 - 1.714)^2 = 0.000169$$

$$(x_2 - \bar{x})^2 = (1.723 - 1.714)^2 = 0.000081$$

$$(x_3 - \bar{x})^2 = (1.688 - 1.714)^2 = 0.000676$$

$$(x_4 - \bar{x})^2 = (1.696 - 1.714)^2 = 0.000324$$

$$(x_5 - \bar{x})^2 = (1.734 - 1.714)^2 = 0.000400$$

3: Sum the squared deviations:

$$\sum(x_i - \bar{x})^2 = 0.000169 + 0.000081 + 0.000676 + 0.000324 + 0.000400 = 0.00165$$

4: Divide by $n - 1$ for the squared standard deviation:

$$\frac{\sum(x_i - \bar{x})^2}{n - 1} = \frac{0.00165}{5 - 1} = \frac{0.00165}{4} = 0.0004125$$

5: Take the square root to find s : $s = \sqrt{0.0004125} \approx 0.0203 \text{ m} \approx 0.02 \text{ m}$

8.2 Processed Data.

To determine velocity decay, I captured a time-series of the projectile's velocity by analyzing successive time frames in Tracker. The high-speed camera recording at 240 fps provided sufficient temporal resolution to track position changes in small time increments. The camera was positioned perpendicular to the plane of motion to minimize parallax distortion, and a meter rule in the frame allowed for accurate distance calibration. After importing the video into Tracker, I plotted the projectile's horizontal velocity against time for each fin configuration. The center of mass of the projectile was manually marked in each frame, and a frame-by-frame analysis was conducted, to ensure a sufficient number of data points were taken for accuracy. Tracker plotted a graph velocity over time, and gave values for velocity at specific time stamps. I was able to find the velocity decay (deceleration) for the projectile by subtracting the final velocity, i.e. 0 as the projectile lands from the velocity at the peak of the projectile, i.e. the maximum velocity and dividing this by the time taken, given by:

$$a = \frac{v_f - v_{\max}}{t} \quad \dots(6)$$

Where: v_f is the final velocity of the projectile (0 ms^{-1}), v_{\max} is the velocity of the projectile at its peak, t is the time taken for the velocity to decrease from its maximum value (v_{\max}) to 0 (v_f) and a is the velocity decay.

1. Calibrating Tracker

As a video gives the dimensions of a body in terms of pixels, calibration associates this information about the pixel in a video to the physical dimensions in the real world (Bharadwaj et al. 3). Thus, the launcher's height was measured to be 30 cm from the desk, and this distance was used as a calibration stick.



Figure 8.2.1 Calibrating Tracker

2. Tracking projectile motion

A point mass target was created for the projectile. Each frame, or step, of the video was searched for the pixels of the projectile. Thus, Tracker plotted the projectile's trajectory.



Figure 8.2.2 Tracking motion

3. Determining velocity decay

Tracker gave the values for instantaneous velocity and time in a data table for an ongoing projectile motion tracking. The velocity increases to a peak then decreases. The velocity decay is how quickly the velocity decreases from this peak (maximum velocity) to 0 (as it lands) per unit time.

Table 8.2 gives calculated Velocity Decay values for each projectile.

Fin length-diameter ratio / L	Velocity decay / a / ms ⁻²						
	Trial 1	Trial 2	Trial 3	Trial 4	Trial 5	Average	Uncertainty
0.00	-1.450	-1.514	-1.435	-1.348	-1.523	-1.454	0.088
0.25	-2.023	-1.842	-1.923	-2.047	-1.946	-1.956	0.103
0.50	-2.546	-2.547	-2.476	-2.691	-2.672	-2.586	0.108
0.75	-2.876	-2.908	-2.869	-2.825	-2.913	-2.901	0.044
1.00	-3.288	-3.137	-3.178	-3.239	-3.189	-3.216	0.076
1.25	-3.489	-3.615	-3.462	-3.560	-3.529	-3.531	0.077
1.50	-4.060	-3.815	-4.001	-4.106	-3.918	-3.980	0.146
1.75	-4.622	-4.479	-4.696	-4.633	-4.480	-4.582	0.109
2.00	-4.926	-4.983	-5.012	-5.030	-5.148	-5.020	0.111

Table 8.2 Velocity Decay

Sample Velocity Decay Calculation for 0.75x fin length:

$$a = \frac{v_f - v_i}{t}$$

$$a = \frac{0 - 3.279}{1.14}$$

$$a = \frac{-3.279}{1.14}$$

$$a \approx -2.876 \text{ ms}^{-2}$$

8.2.1 Uncertainties in Velocity Decay

Sample Uncertainty Calculation for 0.75x fin length:

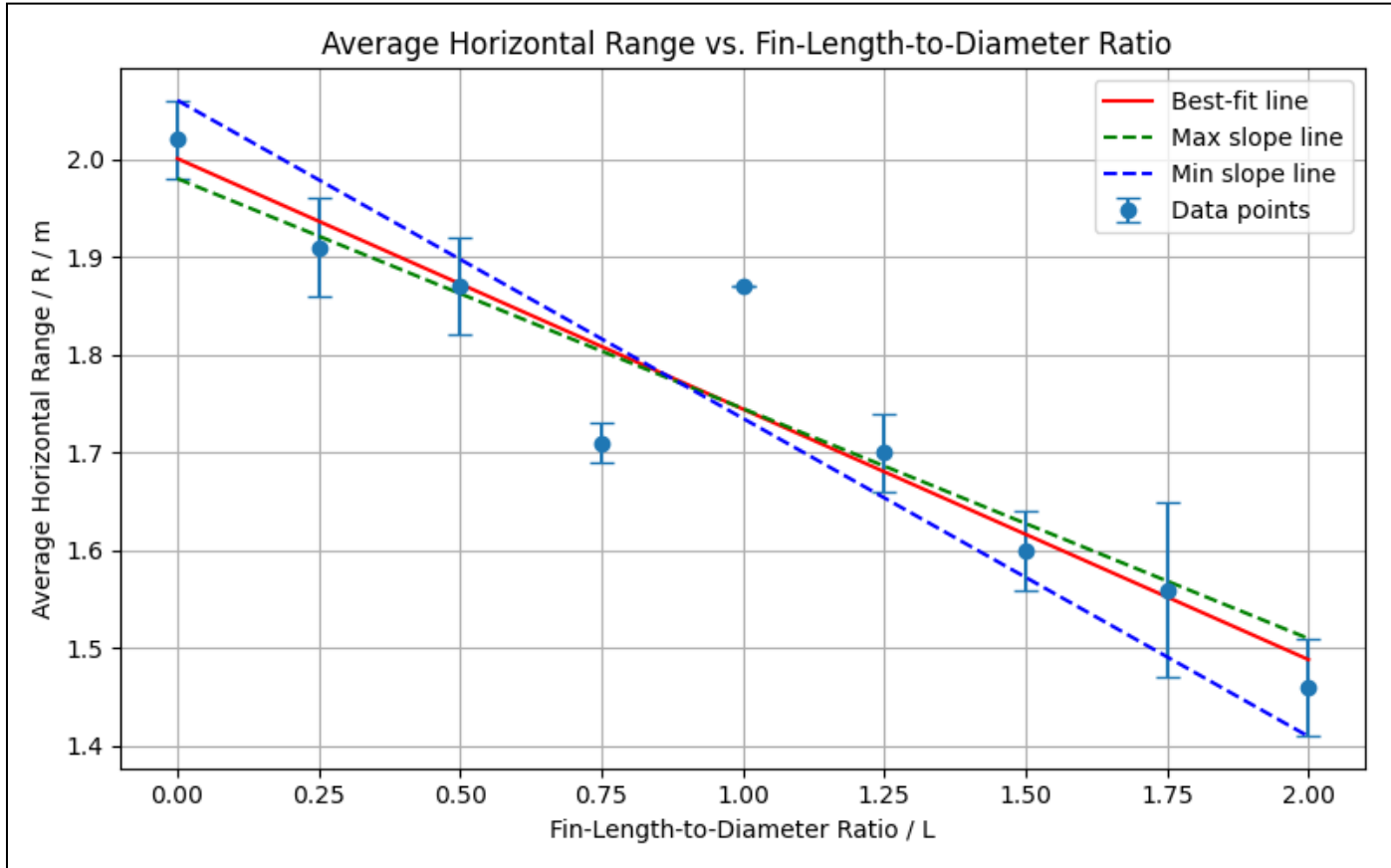
$$\text{Uncertainty} = \frac{\max(\text{Trial Values}) - \min(\text{Trial Values})}{2}$$

$$\text{Trial Values} = \{-2.876, -2.908, -2.869, -2.825, -2.913\}$$

$$\text{Uncertainty} = \frac{-2.825 - (-2.913)}{2} = \frac{0.088}{2} = 0.044 \text{ ms}^{-2}$$

9. Analysis.

9.1 Horizontal Range.



Graph 9.1 Average Horizontal Range vs. Fin Length²

Best-Fit Line: $R = -0.256L + 2.00$

Maximum-Slope Line: $R = -0.235L + 1.98$

Minimum-Slope Line: $R = -0.325L + 2.06$

² Refer to [Appendix 15.6 Uncertainty Calculations](#) for calculations.

We can see a strong negative correlation between fin length and horizontal range observed in the graph indicates that as fin length increases, the horizontal range decreases. The two outlier points will be investigated below. None of the bounding lines approach a slope near zero, so even in a worst-case error scenario we have a clear inverse relationship.

9.2 Investigation of 0.75x and 1.00x outliers.

To determine whether the outliers for 0.75x and 1.00x were not because of random errors, I conducted 5 more trials for each of them. Here are the results:

Fin length-diameter ratio / L	Horizontal Range / R / m					
	Trial 6	Trial 7	Trial 8	Trial 9	Trial 10	New Average
0.75	1.719	1.713	1.720	1.729	1.712	1.719
1.00	1.868	1.886	1.878	1.865	1.875	1.874

Table 9.2 Additional trials for outliers

To explain the anomaly for 0.75x and 1.00x fins, the theories that I came across are:

Boundary Layer Detachment and Vortex Shedding

When air moves past an object with fins, a thin layer of air (boundary layer) sticks to its surface (Shih). However, at certain speeds and angles, this layer can detach (separate) from the surface and later reattach in a different spot. This process happens repeatedly in a cycle.

As a result, swirling air patterns called vortices (small tornado-like air movements) form behind the object. These vortices are shed (released) into the wake, the turbulent region behind the moving object. This shedding of vortices creates rapid pressure changes, which can either increase or decrease the total drag acting on the object (Shih).

For projectiles with fins, these fins provide extra surfaces for the airflow to interact with, which sometimes helps stabilize the wake, reducing drag temporarily. This effect may be most noticeable at specific fin-to-diameter ratios (like 0.75x and 1.00x), where the separation and reattachment of airflow occur in just the right way to unexpectedly lower drag.

Vortex Shedding in Relation to Fin Length

When air flows past an object with fins (like a projectile), vortex shedding occurs. This means that swirling air patterns (vortices) form and break off from the object in a repeating pattern, creating turbulence behind it.

The vortex shedding frequency (f) tells us how often these vortices are released per second. This frequency depends on a value called the Strouhal number (St), which is a number between 0.2 and 0.3 for blunt objects (shapes that aren't streamlined). The equation describing this is ("Strouhal Number"):

$$St = \frac{fL}{v} \dots(7)$$

Where: St is the Strouhal number is a constant for a given shape and flow conditions.. f is vortex shedding frequency; how many times per second vortices are formed. (Hz). L is characteristic length (fin length in this case). v is the velocity of the projectile. Rearranging for f

$$f = \frac{St \cdot v}{L} \dots(8)$$

This means that if the fin length (L) increases, the vortex shedding frequency (f) decreases, in other words, longer fins cause vortices to form less frequently.

For certain fin sizes, like $0.75x$ and $1.00x$ the projectile's diameter, the shedding frequency can reach a resonance-like state. Resonance happens when a system's natural frequency aligns with an external force, causing a stabilizing effect. In this case, it means the projectile moves through the air in a way that reduces turbulence and drag for a short time, allowing it to travel farther than expected.

9.3 Theoretical vs. Experimental Comparisons.

A simple way to quantify the effect of fins is to compare each measured range with the no-drag theoretical range for a 45 degree launch ("3.3: Projectile Motion."):

$$R_{\text{ideal}} = \frac{v_0^2}{g} \dots(9)$$

since $\sin 90 = 1$. To estimate θ , we note that the maximum experimental range (with $0.00x$ control) was approximately 2.02m. Assuming that the no-fins condition is our closest to ideal flight, we can solve for v_0 as follows:

$$2.02\text{m} \approx \frac{v_0^2}{9.8 \text{ ms}^{-2}} \Rightarrow v_0 \approx 4.46 \text{ ms}^{-1}.$$

Substituting $v_0 = 4.46\text{m/s}$ back into yields about 2.02m as the ideal no-drag range.

Fin length-diameter ratio / L	Horizontal Range / R / m	$\Delta R / m$	% Difference
0.00	2.02	- 0.00	- 0.3%
0.25	1.91	- 0.12	- 6.1%
0.50	1.87	- 0.16	- 8.1%
0.75	1.71	- 0.312	- 15.6%
1.00	1.87	- 0.16	- 7.9%
1.25	1.70	- 0.33	- 16.1%
1.50	1.60	- 0.43	- 21.2%
1.75	1.56	- 0.47	- 23.3%
2.00	1.46	- 0.57	- 28.0%

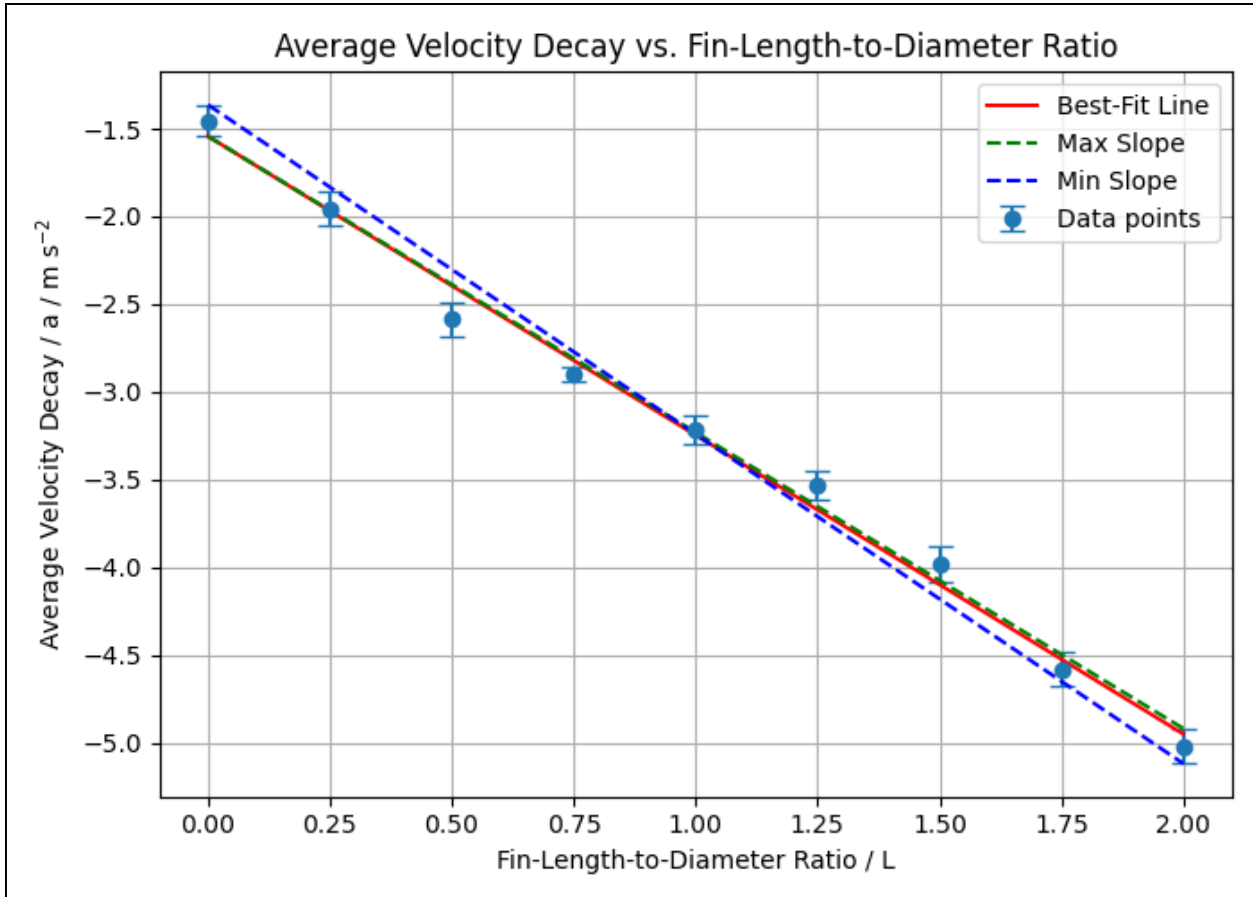
Table 9.3 Percentage Deviation between Experimental & Theoretical Range

Observations:

No-Fins Control (0.00x): The sphere travels 2.023m experimentally, very close to the 2.03m theoretical.

Increasing Fin Length resulting in Larger Range Loss: Even modest fins (0.25 or 0.50 ratio) drop the range by about 6-8%, whereas the largest fins cut range by almost 3%. This supports the hypothesis that fins add significant aerodynamic drag.

9.4 Velocity decay.



Graph 9.4 Velocity Decay vs. Fin Length³

Best-Fit Line: $a = -1.70 L - 1.55$

Maximum-Slope Line: $a = -1.69 L - 1.54$

Minimum-Slope Line: $a = -1.88 L - 1.36$

We see a strong negative correlation between fin length and velocity decay observed in the graph indicates that as fin length increases, the projectile experiences greater aerodynamic drag, leading to greater velocity decay.

³ Refer to [Appendix 15.6 Uncertainty Calculations](#) for calculations.

Comparison with Theoretical Model:

Equation (5) suggests that velocity decay follows an inverse relationship with time, meaning that as time progresses, the rate of velocity loss decreases. However, it does not explicitly predict a linear relationship with fin length. Instead, k (the drag constant) should increase as fin length increases, meaning the decay happens faster for larger fins.

In principle, the model predicts that $\frac{1}{v(t)}$ should increase linearly with time if C_d , ρ , and A remain constant throughout flight. However, two practical considerations arise in my experiment:

Finite Flight Time vs. Theoretical Zero Velocity

Under pure quadratic drag, strictly reaching $v=0$ would require an infinite time. In my tests, the sphere instead collides with the ground in a finite interval; thus, final velocity being 0 is primarily due to the physical impact, not just the drag alone. Consequently, the direct drop from the measured peak velocity to zero in a finite time T is only an approximate match to the formula.

Changing Drag Coefficient in Actual Flight

At higher speeds near launch, flow conditions may differ (e.g., a more turbulent boundary layer) from those near landing, so C_d (and thus k) might not remain strictly constant. This can introduce slight deviations from the neat $1/v$ vs. t linearity that is predicted by Equation (5).

Despite these limitations, my velocity-decay results still provide partial validation of the model: since k is proportional to C_d , A , adding fins increases both the cross-sectional area and the drag coefficient. Experimentally, I observed that as the fin-length-to-diameter ratio increases, the average velocity decay becomes significantly more negative, which is exactly what a larger k would imply.

Equation (5) adequately captures the main phenomenon that velocity decays faster when fins (increasing k) are present. Nonetheless, actual flows around a spherical projectile with fins can have unsteady wake interactions and variable C_d . My data agrees with the quadratic-drag theory (bigger fins \rightarrow bigger drag \rightarrow bigger deceleration), while also showing that full quantitative accuracy would require a piecewise or perhaps a more advanced drag model to accommodate changing flows throughout the flight, something which I could investigate in the future.

Interestingly, while the horizontal range data for 0.75x and 1.00x fin lengths showed anomalies, these anomalies do not appear in velocity decay data, suggesting that factors affecting range and deceleration do not always behave identically.

One possibility is that at intermediate fin lengths, the wake region behind the projectile is stabilized, leading to a temporary reduction in turbulent drag, allowing the projectile to travel farther than expected. The wake region refers to the area of disturbed airflow behind the projectile as it moves through the air. When an object travels, air cannot smoothly wrap around it forever—at some point, the airflow separates from the surface, creating a low-pressure, turbulent zone behind it. This happens because of boundary layer transitions and delayed separation,

meaning that instead of air breaking away from the projectile early (causing a large wake that causes drag), it stays attached for longer, keeping the wake smaller and more stable.

In simpler words, a stable wake smooths the airflow behind the projectile, reducing drag and allowing it to move more efficiently through the air. This is in line with research on boundary layer transitions and delayed separation, which have shown that certain fin geometries can delay flow detachment, momentarily reducing drag coefficients (Bhatia et al.).

The Spearman's rank correlation test was conducted on all the data excluding the two outliers to generate the following heatmap matrix

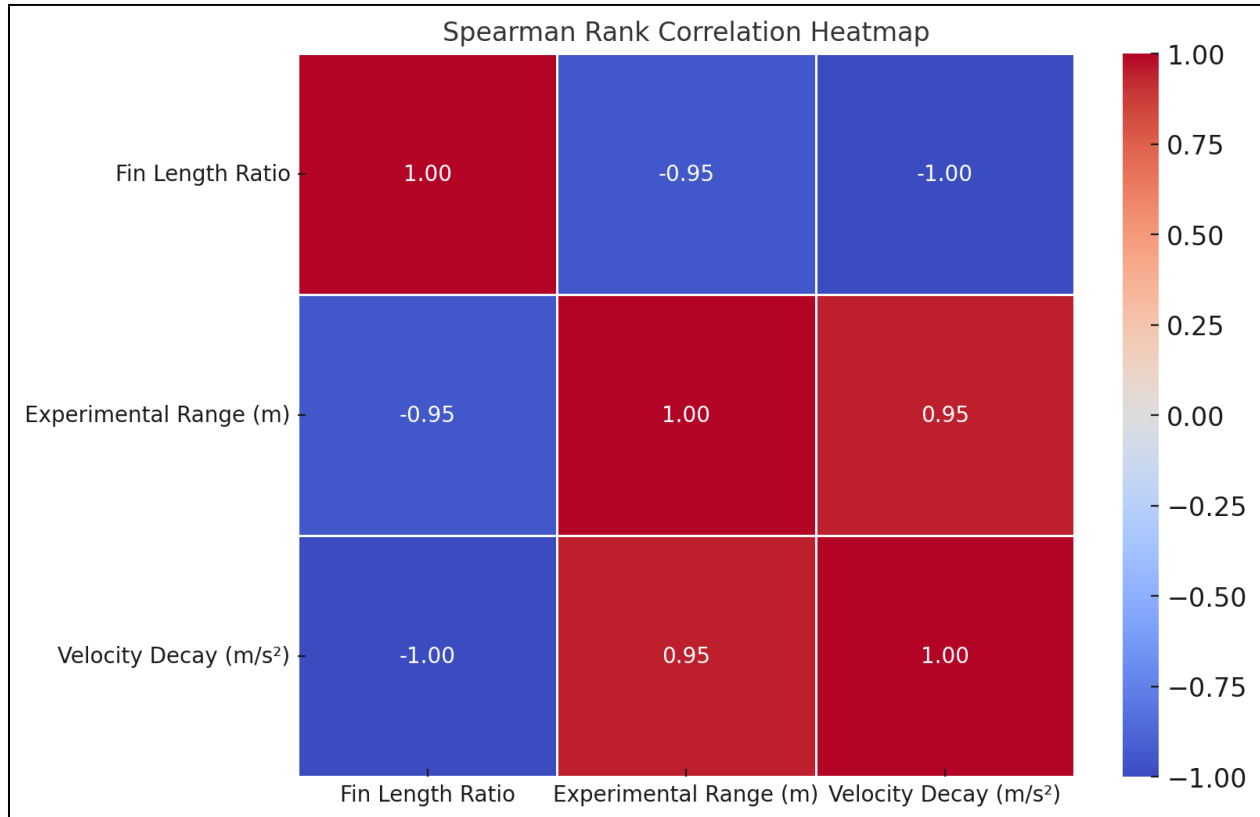


Figure 9.4 Spearman Rank Correlation Heatmap

From this, it can be concluded that as the fin length-to-diameter ratio increases, the velocity decay increases, which aligns with expectations. The strength of this association is strongly positive, indicating that larger fins induce greater aerodynamic resistance, leading to a more rapid loss of velocity. This supports my hypothesis that increased drag caused due to fins plays a significant role in decelerating the projectile over time.

10. Evaluation.

10.1 Limitations.

Although I have treated the drag coefficient (C_d) as effectively constant throughout each

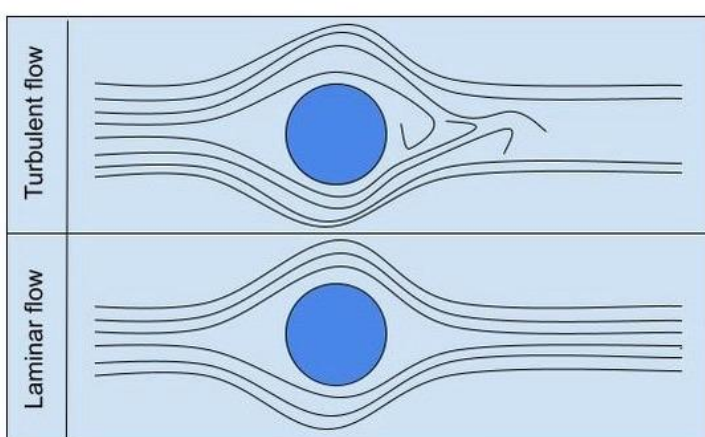


Image 10.1 Turbulent vs. Laminar flow

projectile's flight, this assumption may not be fully accurate for aerodynamic behavior at varying speeds. As the sphere decelerates, the flow conditions change, potentially altering the boundary-layer characteristics and, by extension, C_d of the projectile. At higher initial velocities present near launch, the

flow might be more turbulent, while at lower velocities near impact, the boundary layer could transition to a more laminar flow. Consequently, a single "average" drag coefficient may not accurately translate into the true drag at certain stages of flight. "A Review of the Analysis of Wind-Influenced Projectile Motion in the Presence of Linear and Nonlinear Drag Force."

(Lubarda et al.)⁴ shows that the true drag force often switches between different regimes, linear or nonlinear, depending on factors like flow separation.

10.2 Systematic Errors.

Error	Description	Significance	Improvement
Frame Rate Limitation in Tracker	The limited frame rate of Tracker software may introduce small timing errors in velocity calculations.	Introduces uncertainty in time measurements, affecting velocity decay calculations.	Use a higher frame-rate camera or apply motion filtering to improve accuracy.
Pixel Resolution & Edge Detection	Vibrations make it difficult to accurately define projectile boundaries.	Causes inaccuracies in position measurement of Tracker, affecting range and velocity calculations.	Use higher resolution video capture and calibrate Tracker software for enhanced edge detection.

Table 10.2 Systematic Errors

10.3 Random Errors.

Error	Description	Significance	Improvement
Uncontrolled Minor Air Currents	Minor unpredictable air currents in room can slightly alter projectile motion.	May result in small variations in horizontal range.	Conduct experiments in a wind-isolated environment.
Surface Roughness and Fin Attachment Variability	Irregularities in the application of fin attachment angles may cause unexpected drag effects.	May result in variations in velocity decay and range.	Standardize fin attachment methods application.
Projectile Spin Variability	Projectile spin may vary slightly due to inconsistencies in the launch mechanism, affecting range and velocity decay.	Can alter Magnus effect contributions and lead to minor inconsistencies in trajectory.	Minimize spin by using a controlled launch mechanism.

Table 10.3 Random Errors

⁴ Refer to [Appendix 15.7](#) for comments on Secondary Sources.

11. Conclusion.

The results of my essay strongly uphold the initial hypothesis that increasing fin length on a spherical projectile leads to greater velocity decay and a reduction in horizontal range, chiefly due to greater aerodynamic drag; But to more accurately answer my hypothesis, and investigate the outliers, I would need to find a method to investigate the continuous change of Drag during projectile motion.

12. Further Extension.

In the future, I could explore the impact of fin shape, orientation, and number on drag and stability. Using Computational Fluid Dynamics (CFD) simulations, as employed in "Anomalies in the Flow over Projectiles with Wrap-around Fins" (Krishna et. al) could help visualize wake turbulence and explain the non-linearity observed at mid-range fin lengths in this experiment. Comparing the measured C_d at each fin ratio to a CFD simulation (Yin, Wu, and Lei) would allow us to see if my mid-range anomalies are indeed vortex-induced. With the realisation of so much scope yet to explore, my EE journey has fueled my motivation to pursue aerodynamic studies more than I ever expected.

13. Works Consulted.

1. "3.3: Projectile Motion." LibreTexts. LibreTexts,
[https://phys.libretexts.org/Bookshelves/University_Physics/Physics_\(Boundless\)/3%3A_Two-Dimensional_Kinematics/3.3%3A_Projectile_Motion](https://phys.libretexts.org/Bookshelves/University_Physics/Physics_(Boundless)/3%3A_Two-Dimensional_Kinematics/3.3%3A_Projectile_Motion). Accessed 8 Oct. 2024.
2. "6.07: Drag Force and Terminal Speed." LibreTexts. LibreTexts,
[https://phys.libretexts.org/Courses/Joliet_Junior_College/Physics_201_-_Fall_2019/Book%3A_Physics_\(Boundless\)/6%3A_Applications_of_Newton/6.07%3A_Drag_Force_and_Terminal_Speed](https://phys.libretexts.org/Courses/Joliet_Junior_College/Physics_201_-_Fall_2019/Book%3A_Physics_(Boundless)/6%3A_Applications_of_Newton/6.07%3A_Drag_Force_and_Terminal_Speed). Accessed 8 Oct. 2024.
3. American Society of Mechanical Engineers. Apollo Command Module. Rockwell International Corporation, 1992. Accessed 12 Dec. 2024.
4. Bharadwaj, Jyoti, et al. Analysis of Simple Pendulum Experiment using a PC: An Interactive Approach to Teaching Importance of Errors in Validating Theoretical Models. Central University of Himachal Pradesh, Accessed 12 Feb. 2025.
5. Bhatia, Dinesh, et al. "Transition Delay and Drag Reduction using Biomimetically Inspired Surface Waves." Journal of Applied Fluid Mechanics, vol. 13, no. 4, 2020, pp. 1207–1222, doi:10.36884/jafm.13.04.30316. Accessed 20 Dec. 2024.

6. "Effects of Fins on Drag and Stability of Projectiles." AIAA, 2020. Accessed 10 Jan. 2025.
7. "Turbulence Influence on Finned Projectiles." Journal of Applied Physics, 2021. Accessed 20 Jan. 2025.
8. Clark, Adam M., Jeffrey P. Slotnick, Nigel Taylor, and Christopher L. Rumsey. "Requirements and Challenges for CFD Validation within the High-Lift Common Research Model Ecosystem." AIAA Aviation Forum, 15–19 June 2020, doi:10.2514/6.2020-2772. Accessed 15 Feb. 2025.
9. Homer, David, William Heathcote, and Maciej Pietka. Oxford Resources for IB DP Physics: Course Book. Oxford UP, 2023. Accessed 1 Oct. 2025.
10. Krishna, Ravi, et al. "Anomalies in the Flow Over Projectile with Wrap-Around Fins." Defence Science Journal, vol. 59, no. 5, 2009, pp. 471–484. Accessed 15 Feb. 2025.

11. "Laminar and Turbulent Flow." Vapourtec,
<https://www.vapourtec.com/flow-chemistry/laminar-turbulent/#:~:text=Turbulent%20flow%20is%20a%20flow,the%20tube%20is%20highly%20efficient>. Accessed 5 Jan. 2025.
12. Lubarda, Marko V., and Vlado A. Lubarda. "A Review of the Analysis of Wind-Influenced Projectile Motion in the Presence of Linear and Nonlinear Drag Force." Archive of Applied Mechanics, vol. 92, 2022, pp. 1997–2017. Accessed 15 Feb. 2025.
13. Shih, Chiang. "Flow Over a Circular Cylinder." FAMU-FSU College of Engineering,
<https://web1.eng.famu.fsu.edu/~shih/succeed/cylinder/cylinder.htm>. Accessed 6 Jan. 2025.
14. "Strouhal Number." StudySmarter,
<https://www.studysmarter.co.uk/explanations/engineering/engineering-fluid-mechanics/strouhal-number/>. Accessed 7 Feb. 2025.
15. "Vortex." ScienceDirect,
www.sciencedirect.com/topics/physics-and-astronomy/vortex. Accessed 7 Feb. 2025.

16. "Vortex Shedding." Encyclopedia, MDPI, encyclopedia.pub/entry/32834. Accessed 8 Feb. 2025.

17. Yin, Jintao, Xiaosheng Wu, and Juanmian Lei. "Body-fin interference on the Magnus effect of spinning projectile in supersonic flows." *Engineering Applications of Computational Fluid Mechanics*, vol. 11, no. 1, 2017, pp. 496–512, doi:10.1080/19942060.2017.1319878. Accessed 15 Dec. 2025.

14. List of Figures

1. Stolbovsky. "Vostok 5 reentry capsule 01.jpg." Wikimedia Commons, 5 May 2022, https://commons.wikimedia.org/wiki/File:Vostok_5_reentry_capsule_01.jpg. Accessed 4 Nov. 2024.

15. Appendix.

15.1 Maximum Velocity.

Fin length-diameter ratio / L	Maximum Velocity/ v_{\max} / ms^{-1}					
	Trial 1	Trial 2	Trial 3	Trial 4	Trial 5	Average
0.00	1.088	1.136	1.076	1.011	1.142	1.091
0.25	1.720	1.566	1.635	1.740	1.654	1.663
0.50	2.546	2.547	2.476	2.691	2.672	2.586
0.75	3.020	3.053	3.012	2.967	3.059	3.022
1.00	3.617	3.451	3.496	3.563	3.508	3.527
1.25	4.187	4.339	4.154	4.272	4.235	4.237
1.50	5.075	4.769	5.001	5.133	4.898	4.975
1.75	6.240	6.047	6.340	6.255	6.048	6.186
2.00	7.143	7.226	7.267	7.294	7.465	7.279

Table 15.1 Maximum Velocity

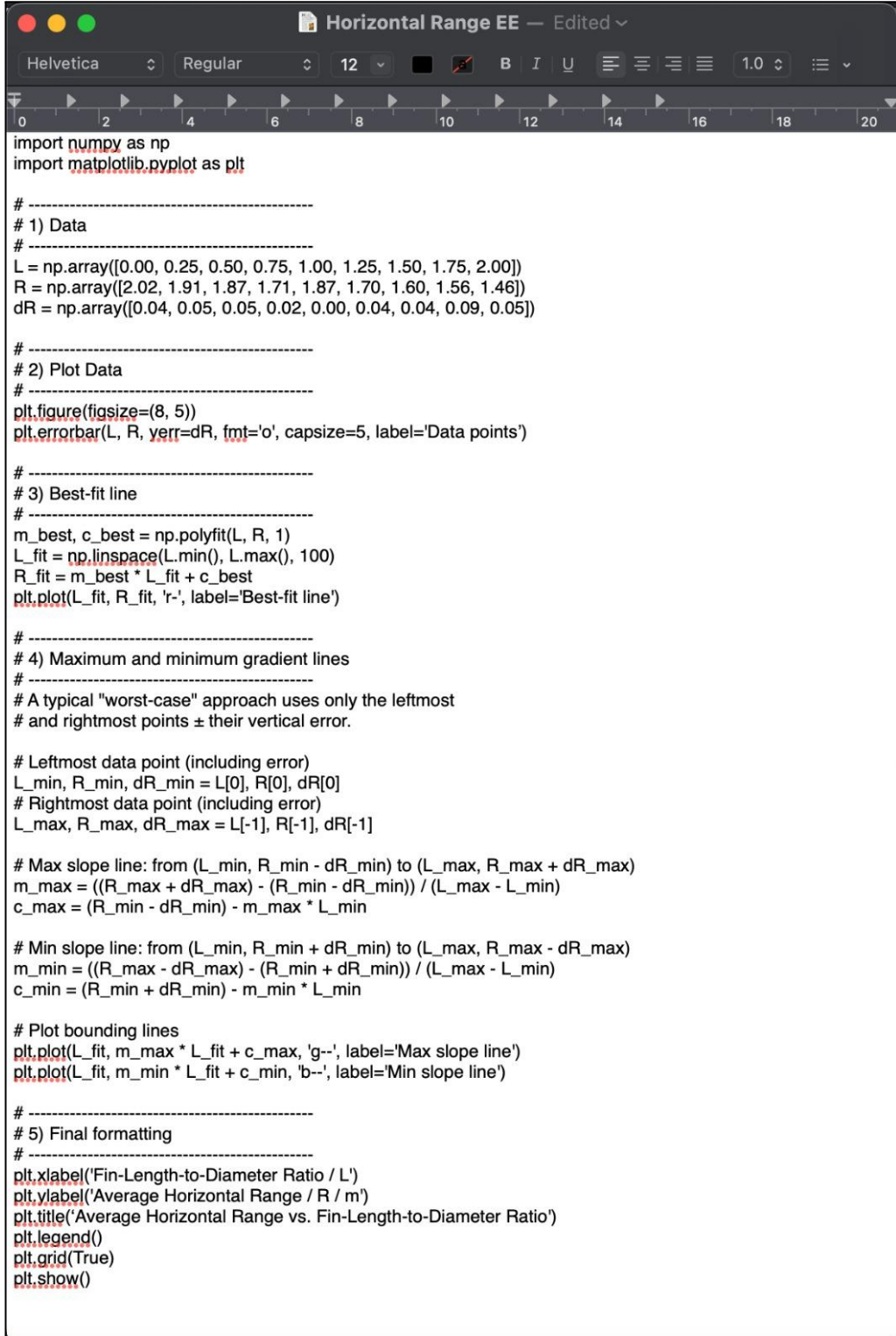
Sample Calculation for Average Maximum Velocity for 0.75x Fin Length:

$$\text{Average Maximum Velocity} = \frac{\sum v_{\max,i}}{N}$$

For Fin Length 0.75x:

$$\begin{aligned} \text{Average Maximum Velocity} &= \frac{(3.020 + 3.053 + 3.012 + 2.967 + 3.059)}{5} \\ &= \frac{15.111}{5} = 3.022 \text{ m/s} \end{aligned}$$

15.2 Python Code for Graph 9.1.



```
Horizontal Range EE — Edited ✓

Helvetica Regular 12 B I U 1.0

import numpy as np
import matplotlib.pyplot as plt

# -----
# 1) Data
# -----
L = np.array([0.00, 0.25, 0.50, 0.75, 1.00, 1.25, 1.50, 1.75, 2.00])
R = np.array([2.02, 1.91, 1.87, 1.71, 1.87, 1.70, 1.60, 1.56, 1.46])
dR = np.array([0.04, 0.05, 0.05, 0.02, 0.00, 0.04, 0.04, 0.09, 0.05])

# -----
# 2) Plot Data
# -----
plt.figure(figsize=(8, 5))
plt.errorbar(L, R, yerr=dR, fmt='o', capsiz=5, label='Data points')

# -----
# 3) Best-fit line
# -----
m_best, c_best = np.polyfit(L, R, 1)
L_fit = np.linspace(L.min(), L.max(), 100)
R_fit = m_best * L_fit + c_best
plt.plot(L_fit, R_fit, 'r', label='Best-fit line')

# -----
# 4) Maximum and minimum gradient lines
# -----
# A typical "worst-case" approach uses only the leftmost
# and rightmost points ± their vertical error.

# Leftmost data point (including error)
L_min, R_min, dR_min = L[0], R[0], dR[0]
# Rightmost data point (including error)
L_max, R_max, dR_max = L[-1], R[-1], dR[-1]

# Max slope line: from (L_min, R_min - dR_min) to (L_max, R_max + dR_max)
m_max = ((R_max + dR_max) - (R_min - dR_min)) / (L_max - L_min)
c_max = (R_min - dR_min) - m_max * L_min

# Min slope line: from (L_min, R_min + dR_min) to (L_max, R_max - dR_max)
m_min = ((R_max - dR_max) - (R_min + dR_min)) / (L_max - L_min)
c_min = (R_min + dR_min) - m_min * L_min

# Plot bounding lines
plt.plot(L_fit, m_max * L_fit + c_max, 'g--', label='Max slope line')
plt.plot(L_fit, m_min * L_fit + c_min, 'b--', label='Min slope line')

# -----
# 5) Final formatting
# -----
plt.xlabel('Fin-Length-to-Diameter Ratio / L')
plt.ylabel('Average Horizontal Range / R / m')
plt.title('Average Horizontal Range vs. Fin-Length-to-Diameter Ratio')
plt.legend()
plt.grid(True)
plt.show()
```

Image 15.2 Code Snippet with comments for Graph 9.1

15.3 Python Code for Graph 9.4.

The screenshot shows a Jupyter Notebook cell with the title "Velocity Decay EE — Edited". The code in the cell is as follows:

```
import numpy as np
import matplotlib.pyplot as plt

L = np.array([0.00, 0.25, 0.50, 0.75, 1.00,
             1.25, 1.50, 1.75, 2.00])
a = np.array([-1.454, -1.956, -2.586, -2.901,
              -3.216, -3.531, -3.980, -4.582, -5.020])
da = np.array([0.09, 0.10, 0.10, 0.04, 0.08,
               0.08, 0.10, 0.10, 0.10])

plt.figure(figsize=(7, 5))

# -----
# 2) Data + Error Bars
# -----
plt.errorbar(L, a, yerr=da, fmt='o', capsized=5, label='Data points')

# -----
# 3) Best-Fit Line
# -----
m_best, c_best = np.polyfit(L, a, 1)
L_fit = np.linspace(L.min(), L.max(), 100)
a_fit = m_best * L_fit + c_best
plt.plot(L_fit, a_fit, 'r', label='Best-Fit Line')

# -----
# 4) Maximum & Minimum Gradient Lines
# -----
L_left, a_left, da_left = L[0], a[0], da[0]
L_right, a_right, da_right = L[-1], a[-1], da[-1]

# Max slope: (L_left, a_left - da_left) → (L_right, a_right + da_right)
m_max = ((a_right + da_right) - (a_left - da_left)) / (L_right - L_left)
c_max = (a_left - da_left) - m_max * L_left
a_max = m_max * L_fit + c_max

# Min slope: (L_left, a_left + da_left) → (L_right, a_right - da_right)
m_min = ((a_right - da_right) - (a_left + da_left)) / (L_right - L_left)
c_min = (a_left + da_left) - m_min * L_left
a_min = m_min * L_fit + c_min

plt.plot(L_fit, a_max, 'g--', label='Max Slope')
plt.plot(L_fit, a_min, 'b--', label='Min Slope')

# -----
# 5) Final Formatting
# -----
plt.title('Average Velocity Decay vs. Fin-Length-to-Diameter Ratio')
plt.xlabel('Fin-Length-to-Diameter Ratio / L')
plt.ylabel('Average Velocity Decay / a / m s^-2')
plt.grid(True)
plt.legend()
plt.tight_layout()
plt.show()
```

Image 15.3 Code Snippet with comments for Graph 9.4

15.4 Python Code for Figure 9.4.

The screenshot shows a Jupyter Notebook cell with the title "Spearman Heatmap EE — Edited". The cell contains the following Python code:

```
import numpy as np
import seaborn as sns
import matplotlib.pyplot as plt

# Correlation matrix
correlation_matrix = np.array([
    [1.00, -0.95, -1.00],
    [-0.95, 1.00, 0.95],
    [-1.00, 0.95, 1.00]
])

# Labels
labels = ["Fin Length Ratio", "Experimental Range (m)", "Velocity Decay (m/s2)"]

# Create heatmap
plt.figure(figsize=(8, 6))
sns.heatmap(correlation_matrix, annot=True, xticklabels=labels, yticklabels=labels,
            cmap="coolwarm", vmin=-1, vmax=1)

# Title
plt.title("Spearman Rank Correlation Heatmap")

# Show the plot
plt.show()
```

Image 15.4 Code Snippet with comments for Figure 9.4

15.5 Experimental Setup.



Image 15.5 Extended view of Experimental Setup

15.6 Uncertainty Calculations

A) Horizontal Range vs. Fin Ratio

Line Equations:

Best-Fit: $R = -0.256 L + 2.00$

Max-Slope: $R = -0.235 L + 1.98$

Min-Slope: $R = -0.325 L + 2.06$

1) Slope Differences (Relative %)

$$\Delta m_{\max} = |-0.256 - (-0.235)| = 0.021 \Rightarrow \frac{0.021}{0.256} \times 100\% \approx 8\%.$$

$$\Delta m_{\min} = |-0.256 - (-0.325)| = 0.069 \Rightarrow \frac{0.069}{0.256} \times 100\% \approx 27\%.$$

2) Intercept Differences

$$\Delta c_{\max} = |2.00 - 1.98| = 0.02, \quad \Delta c_{\min} = |2.00 - 2.06| = 0.06.$$

Thus, while the slope can vary by about 8% (max-slope) to 27% (min-slope) from the best-fit line, and the intercept differs by up to 0.06m, all lines remain still clearly negative.

B) Velocity Decay vs. Fin Ratio

Line Equations:

Best-Fit: $a = -1.70 L - 1.55$

Max-Slope: $a = -1.69 L - 1.54$

Min-Slope: $a = -1.88 L - 1.36$

1) Slope Differences (Relative %)

$$\Delta m_{\max} = |-1.70 - (-1.69)| = 0.01 \Rightarrow \frac{0.01}{1.70} \times 100\% \approx 0.6\%.$$

$$\Delta m_{\min} = |-1.70 - (-1.88)| = 0.18 \Rightarrow \frac{0.18}{1.70} \times 100\% \approx 10.6\%.$$

2) Intercept Differences

$$\Delta c_{\max} = |-1.55 - (-1.54)| = 0.01, \quad \Delta c_{\min} = |-1.55 - (-1.36)| = 0.19.$$

Even with the extremes, the slope remains considerably negative in all cases, confirming that larger fin ratios do result in more negative (i.e.faster) velocity decay.

15.7 Secondary Sources.

The type of secondary sources used in the Essay are displayed in Chart 10.5. Journals and Reports contribute 64%, thus almost 65% of sources are published and verified literature, which are referenced for comparison and validation with the results of my EE. The Journals' publication dates

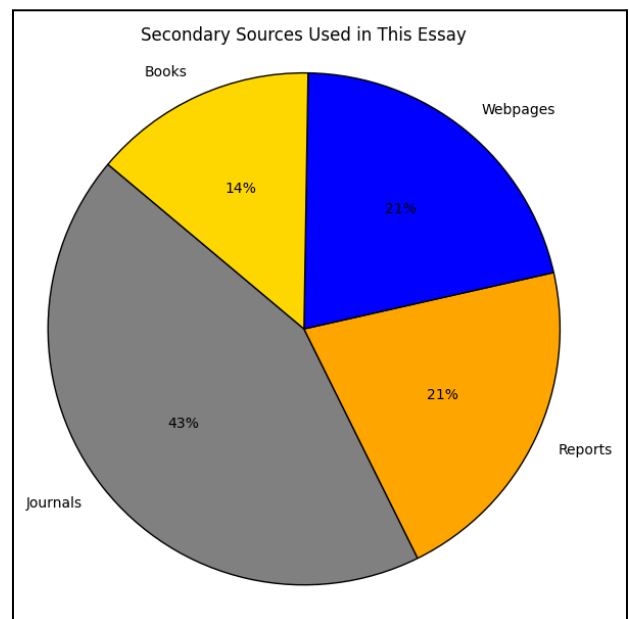
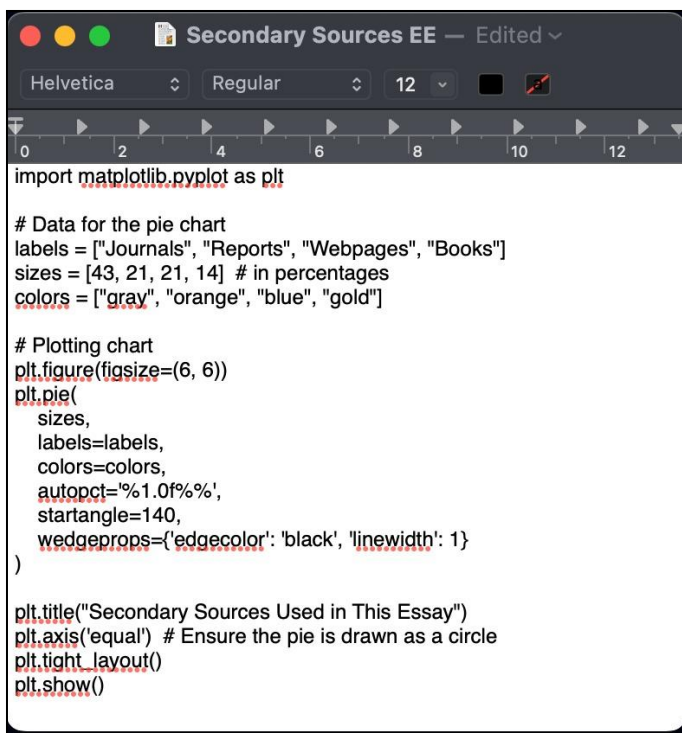


Chart 15.7 Secondary Sources

(2020–2022) make them quite relevant, as aerodynamic research is advancing rapidly. Although the 1992 Apollo Command Module Report might seem dated, it is directly relevant as the revolutionary Apollo program's engineering principles remain a valuable historical precedent for spherical or capsule-type designs that are still used to this date.

Web pages at 21% were used in conjunction with books to check standard aerodynamic concepts and cross-referencing them with textbooks or journals to ensure accuracy. They were used as a



```
import matplotlib.pyplot as plt

# Data for the pie chart
labels = ["Journals", "Reports", "Webpages", "Books"]
sizes = [43, 21, 21, 14] # in percentages
colors = ["gray", "orange", "blue", "gold"]

# Plotting chart
plt.figure(figsize=(6, 6))
plt.pie(sizes,
        labels=labels,
        colors=colors,
        autopct='%.1f%%',
        startangle=140,
        wedgeprops={'edgecolor': 'black', 'linewidth': 1})
plt.title("Secondary Sources Used in This Essay")
plt.axis('equal') # Ensure the pie is drawn as a circle
plt.tight_layout()
plt.show()
```

'connection' bridge for knowledge and understanding between Books (14%) and Journals and Reports.

Overall, I am content with the breadth of published literature that I mostly used in the latter half of my essay complemented with a bit of online and textbook material that I used as the beginning base during the initial stages of my EE.

Image 15.7 Code Snippet with comments for Chart 15.7